International Journal Of
Industrial Electronics Control and Optimization
Print ISSN: 3517-2645
Online ISSN: 3568-2645
Homepage: https://ieco.usb.ac.ir/

# Virtual Inertia Control and Small-Signal Stability Analysis of Electric Vehicle

Mehran Jami

Department of Electrical Engineering, Islamic Azad University, Marivan Branch, Marivan, Iran
Corresponding author's email: mehran.jami8@gmail.com

**Article Info**

**Article type:**
Research Article

**Article history:**
Received: 24-July-2023
Received in revised form: 21-September-2023
Accepted: 26-October-23
Published online: 30-October-23

**Keywords**:
Electric Vehicle, Energy Storage System, Small-Signal Model, Stability, Virtual Inertia

**ABSTRACT**

In electric vehicles (EVs), the small size of the dc link capacitor results in significant voltage deviations when there are changes in load or uncertain fluctuations from the power resources. This causes a decline in voltage quality. To address the issue of low inertia, this study suggests the use of a fast-responding energy storage system, such as a supercapacitor (SC), which can replicate inertial responses through a specified control algorithm. A virtual capacitor and a virtual conductance are presented in this paper, which are implemented in the inner loop control, specifically the current loop control of SC, to effectively emulate inertia and damping and improves the battery lifetime by reducing the rate of charge and discharge. To assess the stability of the EV, a comprehensive small-signal model is developed, and the acceptable range of inertia response parameters is determined through eigenvalues analysis of the system. Numerical simulations are conducted to demonstrate the performance of the proposed control structure.

## I. Introduction

The energy storage system utilized in electric or hybrid vehicles remains a major challenge due to its high cost, limited range, and slow recharge times. Therefore, the primary focus for advancing electric vehicles lies in enhancing onboard energy storage systems to improve range, size specifications, and lifespan [1]. The concept of electric vehicles (EVs) emerged with various energy storage devices such as batteries, fuel cells (FCs), and ultracapacitors (UCs) or supercapacitors (SCs). Modification of these EVs led to the development of hybrid electric vehicles (HEVs), combining the aforementioned sources to enhance efficiency and ensure uninterrupted power supply in vehicles [2]. A combination of fuel cell and battery is proposed in [3]. A similar study on SC and fuel cell is proposed in [4] and a study on fuel cell, SC and battery is proposed in [5]. Energy sources are fully responsible for supplying the required load of hybrid electric vehicles (HEVs) at different voltage levels according to different vehicle speeds. To ensure the correct operation of electronic equipment, it is necessary to adjust the main DC bus voltage. Power converters play a vital role in transportation industry to achieve dynamic voltage regulation and maintain coupling between energy sources and three-phase induction motor. Therefore, various types of power converters have been presented in the past. Many control algorithms for HEV energy management and control have been proposed in previous studies. For efficient energy management, predictive controllers have been proposed for energy control among fuel cells, SC, and batteries [6]. A fuzzy logic controller based on genetic algorithms is introduced to improve the performance and fuel economy of his fuel cell-based HEV [7]. Adaptive fuzzy logic-based controllers are used for energy management in his fuel cell and battery-based HEVs, controlling performance and maintaining battery state of charge [8]. Additionally, a predictive control model was introduced to improve battery performance and prevent battery and fuel cell degradation [9]. According to the various methods that have been presented in the field of using energy storage resources in a hybrid electric vehicle and its control, it is clear that in these methods, the control objectives considered include improving the inertia of the DC microgrid in the form of

Copyright © Jami et al.
Published by University of Sistan and Baluchestan.

reducing the rate of change of voltage (RoCoV) immediately after the change, the increase in DC link voltage response damping, and also the improvement of DC microgrid stability in the presence of constant power loads (CPLs), have not been studied at the same time.

The electric vehicle is an unconventional power system that differs from traditional ones with rotating machines. It is a DC microgrid (DC-MG) that is predominantly controlled by power electronics and can operate independently. By integrating electric vehicles with local renewable sources and loads, the foundation for microgrids involving EVs can be established [10]. The presence of native DC sources like photovoltaic systems and EV batteries facilitates the creation of DC microgrids, which have a shared DC link and can connect to the AC low-voltage network of the local distributor [11]. The inclusion of a bidirectional DC converter (Bi-C) is crucial in linking parallel-energy storage units (ESUs) to the dc buses and achieving voltage conversion. This design characteristic renders the EV a system without inertia [12]. Furthermore, from the perspective of the source bus, a power electronic converter behaves like a constant power load when it precisely regulates its output voltage with a resistance load. Despite having a negative incremental impedance, the CPL has a positive instantaneous impedance. As a result, the system's damping is reduced and its susceptibility to oscillation is increased [13]. In summary, the stability of EV, like other islanded DC-MGs, is at risk due to its negative impedance and low inertia characteristics [14]. This poses a challenge to the reliable and convenient power supply for EVs, ultimately impeding the widespread adoption of electric vehicles. Consequently, it is necessary to enhance the dynamic voltage stability of EV in order to ensure efficient and high-quality charging of EVs [15]. A suggestion has been made in [16] to improve the frequency stability of an islanded MG by using a hybrid ESS (HESS) consisting of both a SC and an electric vehicle battery. Authors in [17] present a method for frequency stabilization of the utility grid by modulating the power level of an inductive electric vehicle charger supplied by the grid. To replace the greater damping coefficient, Huang *et al.* [18] create a dynamic virtual impedance (DVI) based on the damping mechanism of the damping torque analysis. A modified droop control method using Neuro-Fuzzy Inference System (ANFIS) [19] and fuzzy logic [20] are designed based on the inertia injection, which injects adaptive virtual inertia instead of modeling the constant inertia. The work mentioned above, however, focuses on AC-MG rather than DC-MG. A simple method to improve system inertia in DC-MG, such as EV, is adding extra capacitors. These capacitors utilize their stored energy to counteract the rapid fluctuations in voltage. However, it should be noted that while this approach enhances system performance, it also requires additional investment and poses challenges in terms of limited space availability [15]. In [21], the virtual inertia is adaptively adjusted to enhance the stability of the DC-MG by establishing the relationship between the inertia coefficient and rate of change of voltage. In [15], strategies for enhancing the dynamic stability and ensuring a high-quality power supply for electric vehicles are discussed. These strategies, known as inertia droop control (IDC), are specifically designed for bidirectional dc converters. Unlike the virtual inertia and damping control (VIDC), the proposed IDC offers a simpler solution by making slight modifications to the conventional droop control method, eliminating the need for intricate control structures. In comparison to the VIDC discussed in previous literature [22], which was derived using a complex machine model, the simplified control structure of the inertia droop control (IDC) offers greater convenience for practical application and promotion in DC-MG. Additionally, IDC also addresses the voltage deviation issue inherent in droop control, a problem that was not previously considered in the literature The stability mechanism of VIDC has not been extensively explored in previous literature. Typically, the impedance-based method is used to investigate stability mechanisms and evaluate voltage stability [23]. In [22], a feedback analytic approach is introduced to analyze the PD caused by virtual DC machine control, which explains how the voltage behaves when subjected to disturbance current. However, this approach still relies on impedance-based analysis, solely focusing on the port characteristics. The stability of a DC network designed for electric vehicle charging stations (EVCSs) was examined by the authors of [24]. The purpose of this investigation is to provide general recommendations for network planning by demonstrating how the interconnection of EVCSs may affect the stability of the DC network.

According to the various methods that have been presented in the field of using energy storage resources in an electric vehicle and its control, it is clear that in these methods, the control objectives considered include improving the inertia of the DC network in the form of reducing the rate of change of voltage immediately after the change, the increase in DC link voltage response damping, and also the improvement of DC network stability in the presence of CPLs, have not been studied at the same time. Therefore, this research gap is covered in this study. To address the gaps in the existing literature, a virtual impedance control loop including virtual capacitor and virtual resistance by using the virtual inertia concept is proposed in this paper. The salient features of this work can be summarized as:

- Comprehensive modeling of an electric vehicle in the form of a DC microgrid including distributed generation sources, interface converters and loads connected to a common DC link.
- Small signal stability analysis of DC microgrids independent from the main grid considering CPLs and proposed virtual inertial control.

- Investigating the influence of CPLs on the stability of low frequency dominant modes of the studied DC microgrid.
- Improving the dynamic behavior of common DC link voltage by using the proposed virtual inertial control loop.
- The use of SC as a suitable source of energy storage for quick injection of virtual inertia immediately after disturbance.
- The size of capacitors in EV is usually small, because these elements have a large impact on short-circuit current, system reliability, and control system complexity. The use of large capacitors causes problems in the field of fault detection, fault isolation and system protection. Also, the use of large capacitors increases the cost, weight, and volume of the entire system. Increasing the DC link capacitor virtually, using energy storage source and appropriate control method is investigated as the main goal of this research.

The rest of this paper is organized as follows. In Section II, the proposed structure of electric vehicle is introduced. Section III describes the small-signal model of electric vehicle. The stability analysis of the system in the presence of the proposed controller are presented in Section IV. Simulation results are presented in Section V and Section VI concludes the paper.

## II. Structure of The Proposed electric Vehicle

Fig. 1 shows the structure of the electric electrical vehicle studied in this research. The battery and SC units are charged or discharged according to the power requirements and working conditions of the vehicle. The solar panel is also controlled based on the tracking of the maximum power point and according to the weather conditions, the maximum power can be produced. The loads in the vehicle are divided into three general categories. The main part of the energy consumed in the car is related to the wheels and the propulsion power that moves the vehicle. For this purpose, we have considered four three-phase induction motors that are placed on the wheels, and connected to the AC link. Other non-motorized AC loads are also assumed to be connected to the AC link. Other loads are considered as DC loads which are connected to the DC link of the system. In order to better control and manage energy consumption each of the auxiliary energy sources is used to connect to the common DC link from an interfaced power electronic converter. In the following, we will study each of these parts in more detail and examine the different working modes of the vehicle.

### *A. Battery Unit*

Lithium-ion batteries with high energy density are the best choice for storing energy in electric vehicles. However, the high charging and discharging cycles that is required during the operation of the vehicle reduces the life of the battery. The main structures for connecting energy storage sources to the DC link are divided into two categories: 1) passive structure and 2) active structure. The passive structure has the simplest structure in which the sources are directly connected to the DC

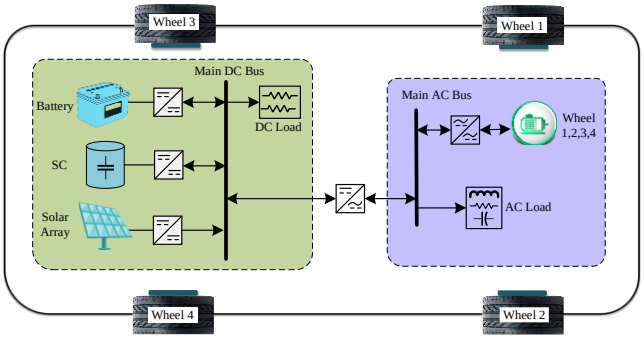



Fig. 1. Structure of the proposed eelctric vehicle.

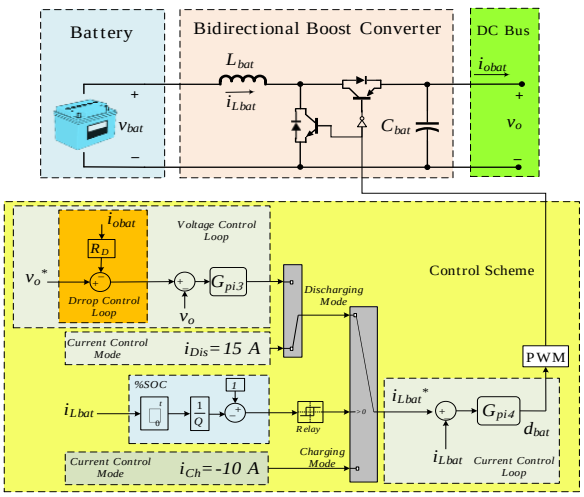


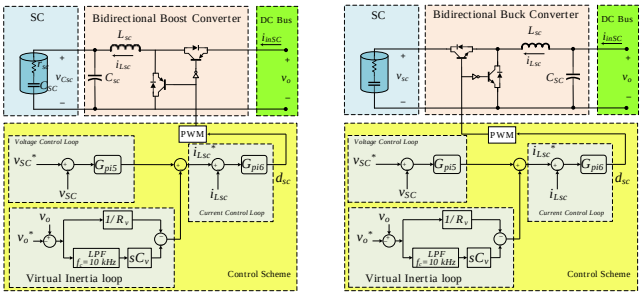

Fig. 2. Configuration and control diagram of battery unit.

link without an intermediary, and the degree of freedom of its control is zero, and no control algorithm is used in this structure. The charging and discharging control of each power source is obtained based on the value of internal resistance of them. In this method, the battery and other energy sources cannot be used effectively. Although this method is simple and inexpensive, its efficiency is often far from expected. In the active structure, a DC-DC interface converter is used to connect the battery to the DC link. Another great advantage of this interface boost converter is the ability to create a variable DC link voltage. The battery interfaced converter is bidirectional, which makes the power return to the battery in braking mode and charges the battery through the high voltage DC link. In the powertrain of electric vehicles, the output voltage of the battery is in the range of 800 V. The proposed power and control systems for the battery unit is shown in Fig. 2. In general, the battery operates in charging or discharging modes. By calculating the state of charge (SOC), it is determined whether the battery has enough charge or not. If the battery charge is less than the specified range, the charging mode is activated and it is charged through the DC link and other sources connected to this link. In this case, the battery operates in the current control mode with a fixed current value and remains in this mode until it reaches the specified full

charge level. When the battery is fully charged, it goes into discharge mode. According to the system conditions, the battery can be operated in current control or voltage control mode. In the current control mode, the battery is discharged with a constant current and the main DC voltage will be controlled by other units. In addition, if the main source, i.e., the internal combustion engine, is turned off and the vehicle works in full electric mode, the battery operates in voltage control mode and it is responsible for controlling the DC link voltage.

### B. Supercapacitor Unit

With the rapid expansion of electric vehicle applications in recent decades, the dynamic performance, cost, and durability of hybrid vehicles still largely depend on the design, component integration, and control of energy storage systems. The high price and short lifetime of pure battery systems are the biggest obstacles to the further adoption of electric vehicles. Energy storage systems are the main components of electric vehicles, which have a great impact on efficiency, driving distance and performance of vehicles. In electric vehicle the size of the battery is obtained based on the characteristics of the vehicle driving distance. The power density of batteries is very low compared to their energy density, and their equivalent series resistance is in the range of several hundred milliohm. Therefore, operating the battery at high power may cause large losses and shorten the lifespan. A simple solution to increase power capacity and reduce losses in energy storage systems is to use a larger battery pack. Although the energy capacity required to transport passengers is close to 100 kWh, a trade-off between weight, driving distance, performance and cost must be considered. Doubling the size of the batteries does not necessarily lead to a linear increase in the driving distance [25]. A solution that prevents the installation of large battery sets is the use of hybrid storages, which a source with high power density is used together with a high energy density battery. SC are the most developed technology in high power, short consumption and light weight applications due to their power density several thousand times larger than lithium-ion batteries. They are less exposed to extreme temperature increase and can be easily connected to power electronic converters in the propulsion system. The design of the battery pack is based on the energy required to travel a certain distance and the capacitor bank is designed as a power source to provide acceleration and power requirements. Fig. 3 shows the structure of the SC, bidirectional DC-DC interface converter, and its control system. The SC is connected to the common DC link through the power electronic converter. To show the generality of the proposed control method and is not dependent on the type of interface converter, two different DC-DC converters, buck and boost interface have been studied. The converters under study are considered to be bidirectional so that they pass current in both directions and the SC works well in charge and discharge modes. The proposed control circuit




(a) (b)

Fig. 3. Configuration and control diagram of SC unit, a) interface boost converter, b) interface buck converter

consists of three different loops. The voltage control loop is responsible for regulating the voltage of the SC and returns it to the nominal value in the charging and discharging modes. The proposed control loop is a virtual inertial loop. In DC microgrids, the size of the DC link capacitor is too small to provide inherent inertia to the system. As a result, in case of load changes or power fluctuations on the side of production sources, large and rapid voltage changes will occur in the DC link, which leads to a decrease in the quality of the system voltage. Energy storage systems are used to provide better performance, improved inertia and dynamic stability of the electric vehicle.

### C. PV Unit

The output power generated from the solar panel is very low to drive the powertrain in electric vehicle. Therefore, solar energy is used as an auxiliary source to reduce energy consumption from batteries and fuel sources and is used to charge batteries when needed. Evaluating the installation of solar arrays on the roof of cars, tracking the maximum power point to quickly track changes in conditions, and analyzing the effects of solar panels on improving the distance traveled are the challenges that exist in the development of solar panel-based car applications. In [26], the authors have presented the fuel cell/battery/solar panel structure in which the maximum power point tracking algorithm has not been considered. Therefore, for better performance of the solar panel and tracking the maximum power point (MPP), a unidirectional boost converter has been used. By applying the appropriate control method, the solar cell works at a specific voltage and current where the output power of the system is maximum for a given conditions. Fig. 4 shows the structure of the PV, unidirectional DC-DC interface converter, and its control system.

### D. AC and DC Loads

The loads in electric vehicle can be considered as direct current (DC) loads connected to the common DC link and alternating current (AC) loads connected to the AC link. Most of the energy in hybrid cars is consumed by AC loads or the induction motors installed inside the wheels, which are responsible for moving the vehicle. In addition to this, there

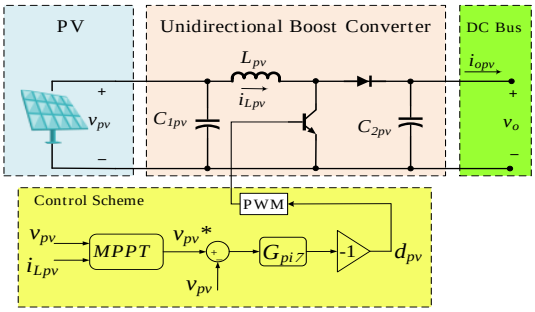



Fig. 4. Configuration and control diagram of PV unit.

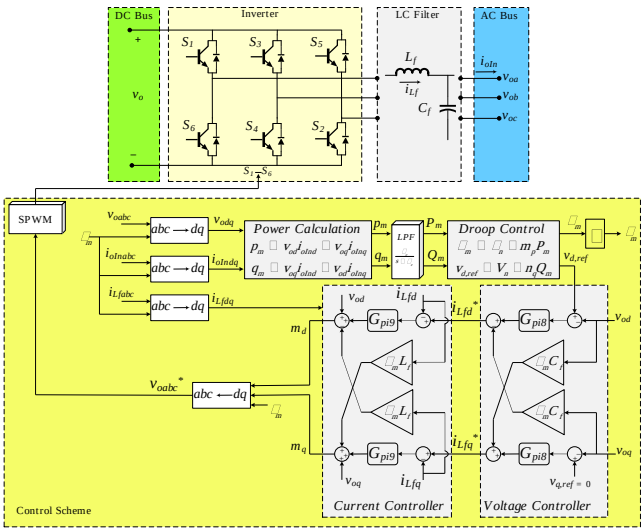



Fig. 5. Configuration and control diagram of inverter unit.

are internal loads and other loads when the cars are in parking mode and their collection provides the camp's energy needs in the form of a microgrid. Therefore, the existing loads are divided into two parts: motor loads and fixed impedance loads. The constant impedance loads connected to the DC link are assumed as pure resistance and the constant impedance loads connected to the AC link are assumed to be a combination of resistance, inductor and capacitor in series. An inverter with sinusoidal pulse width modulation is used to create an AC link with controllable constant voltage and frequency. By applying a suitable control method, the DC input of the inverter, which is connected to the DC link, is converted into a three-phase sine wave form with a certain voltage and frequency, and makes a controllable three-phase AC link available, which can be used to drive motors through this link. The three-phase induction fed the wheels as well as other AC loads. Fig. 5 shows the structure of the inverter and its related control circuit.

## III. Small-Signal Modeling of Electric Vehicle

In this section, a detailed small-signal model of the EV system is obtained to demonstrate the effectiveness of the proposed method and to investigate the behavior of the system in the presence of energy storage devices and loads. In terms of small-signal stability, hybrid vehicle operation in pure electric mode is the worst-case scenario. Therefore, small-signal stability analysis has been investigated for this mode. Also, in this section, without loss of generality and for the simplicity of calculations, the internal resistances of the inductor and the line have been neglected.

### A. Small-Signal Model of The Battery Unit

For the bidirectional boost converter between source bus (360 V) and main dc bus (800V) if the switch turns on, it yields

$$\begin{cases} L_{bat}\dfrac{di_{Lbat}}{dt} = v_{bat} \\ C_{bat}\dfrac{dv_o}{dt} = -i_{obat} \end{cases} \quad (1)$$

where $i_{Lbat}$, $v_o$ and $i_{obat}$ are the inductor current, the output voltage, the output current, respectively. If the switch turns off, it yields

$$\begin{cases} L_{bat}\dfrac{di_{Lbat}}{dt} = v_{bat} - v_o \\ C_{bat}\dfrac{dv_o}{dt} = i_{Lbat} - i_{obat} \end{cases} \quad (2)$$

By using state-space averaging, the state-space function is derived as

$$\begin{cases} L_{bat}\dfrac{di_{Lbat}}{dt} = v_{bat} - (1-d_{bat})v_o \\ C_{bat}\dfrac{dv_o}{dt} = (1-d_{bat})i_{Lbat} - i_{obat} \end{cases} \quad (3)$$

where $d_{bat}$ is the duty cycle for on-state of the switch. Based on the results given in (3), the small-signal model is achieved as

$$\begin{cases} L_{bat}\dfrac{d\hat{i}_{Lbat}}{dt} = \hat{v}_{bat} - D'_{bat}\hat{v}_o + \hat{d}_{bat}V_o \\ C_{bat}\dfrac{d\hat{v}_o}{dt} = D'_{bat}\hat{i}_{Lbat} - \hat{d}_{bat}I_L - \hat{i}_{obat} \end{cases} \quad (4)$$

where the variables appear in capital letter represent the steady-state values and the variables with "^" indicate the small-signal deviation. Meanwhile, $D'_{bat}=(1-D_{bat})$ By considering the control diagram in Fig. 3 and assuming power sharing loop is off ($R_d = 0$), the small signal model in frequency domain is achieved

$$\hat{d}_{bat}(s) = \hat{v}_o^*(s)G_{pi3}G_{pi4} - \hat{v}_o(s)G_{pi3}G_{pi4} - \hat{i}_{Lbat}(s)G_{pi4} \quad (5)$$

By integrating the two equations (4) and (5) it yields

$$\hat{v}_o(s) = G_{11}.\hat{v}_{bat}(s) + G_{12}.\hat{v}_o^*(s) - Z_{o1}.\hat{i}_{obat}(s) \quad (6)$$

where

$$G_{11} = \frac{D_{bat}^{\prime 2} + I_{Lbat}G_{pi4}}{T_1}, Z_{o1} = \frac{L_{bat}s + V_{bat}G_{pi4}}{T_1},$$
$$G_{12} = \frac{(V_oD_{bat}^{\prime} - I_{Lbat}L_{bat}s)G_{pi3}G_{pi4}}{T_1}$$

$$T_1 = D_{bat}^{\prime 2} + L_{bat}C_{bat}s^2 + G_{pi3}G_{pi4}(V_oD_{bat}^{\prime} - I_{Lbat}L_{bat}s) + G_{pi4}(V_oC_{bat}s + D_{bat}^{\prime}I_{Lbat}). \quad (7)$$

For the bidirectional boost converter used for SC, the analysis is presented in the next subsection.

### B. Small-Signal Model of The Supercapacitor Unit

For the bidirectional boost converters used for SC, the converter topology is shown in Fig. 3. In order to avoid repetition, no detailed procedure is shown below. By using the similar procedure in III-A, one can obtain the final small-signal model of the boost converter as

$$\begin{cases} L_{SC}\dfrac{d\hat{\imath}_{Lsc}}{dt} = D_{SC}\hat{v}_o + V_o\hat{d}_{sc} - \hat{v}_{Csc} \\ C_{sc}\dfrac{d\hat{v}_{Csc}}{dt} = \hat{\imath}_{LSC} - \hat{\imath}_{SC} \\ C_{SC}\dfrac{d\hat{v}_{CSC}}{dt} = \hat{\imath}_{SC} \\ \hat{\imath}_{inSC} = D_{SC}\hat{\imath}_{LSC} + I_{LSC}\hat{d}_{sc}, \hat{\imath}_{SC} = \dfrac{\hat{v}_{Csc} - \hat{v}_{CSC}}{r_{SC}} \end{cases} \quad (8)$$

where $i_{Lsc}$, $v_{CSC}$, $v_{Csc}$ and $d_{sc}$ are the inductor current, the SC voltage, the capacitor voltage, the duty cycle for on-state of the switch, respectively. A virtual capacitance and resistance control strategy is implemented in inductor current loop as follows

$$\hat{i}_{LSC}^{\ *} = C_v\frac{d\hat{v}_o}{dt} + \frac{1}{R_v}\hat{v}_o \quad (9)$$

where $C_v$ and $R_v$ are the virtual capacitance and virtual resistance, respectively. Because the proposed control is at the inner current control loop, it needs to be faster than the outer voltage level control. This control also ensures a rapid response to changes in load, providing fast inertia response. The equation (9) demonstrates that the rate of voltage change ($d\hat{v}_o/dt$) and voltage deviation ($\hat{v}_o$) decrease when $C_v>0$ and $0<R_v<1$ during load changes. This leads to an improvement in the inertia and damping of the EV. Fig. 3 illustrates the implementation of the proposed inertia response control loop within the inner current control loop. However, it should be noted that the pure differentiation of the virtual capacitance in the proposed inertia response strategy may introduce unwanted high frequency noises to the system. A first-order low-pass filter (LPF) is constructed in series with the virtual capacitance feedback to solve this problem. By considering the control diagram in Fig. 3, the small signal model in frequency domain is achieved

$$\begin{aligned} \hat{d}_{sc}(s) = {} & \hat{v}_o(s)G_{pi6}(C_v s G_{LPF} + 1/R_v) - \hat{i}_{LSC}(s)G_{pi6} \\ & - \hat{v}_o^*(s)G_{pi6}(C_v s G_{LPF} + 1/R_v) - \hat{v}_{Csc}(s)G_{pi5}G_{pi6} \end{aligned} \quad (10)$$

By analyzing the simultaneous equations of (8) and (10), it yields

$$\hat{v}_o(s) = G_{21}.\hat{v}_o^*(s) + Z_{in,SC}\hat{I}_{inSC}(s) \quad (11)$$

where

$$\begin{aligned} & G_{21} = \frac{V_o G_{pi6}\left(C_v s G_{LPF} + 1/R_v\right)}{T_3}, \\ & Z_{in,SC} = \frac{(L_{SC}s + V_o G_{pi6})T_2 + (1 + r_{SC}C_{SC}s)(1 + V_o G_{pi5}G_{pi6})}{T_2 T_3 D_{SC}} \\ & T_2 = (C_{sc} + C_{SC})s + r_{SC}C_{sc}C_{SC}s^2 \\ & T_3 = D_{SC} + V_o G_{pi6}\left(C_v s G_{LPF} + 1/R_v\right). \end{aligned} \quad (12)$$

For the unidirectional boost converter used for PV, the analysis is presented in the next subsection.

### C. Small-Signal Model of The PV Unit

For the unidirectional boost converters used for PV, the converter topology is shown in Fig. 4. In order to avoid repetition, no detailed procedure is shown below. By using the similar procedure in III-A, one can obtain the final small-signal model of the boost converter as

$$\begin{cases} L_{pv}\dfrac{d\hat{\imath}_{Lpv}}{dt} = \hat{v}_{pv} - D_{pv}^{'}\hat{v}_o + V_o\hat{d}_{pv} \\ C_{2pv}\dfrac{d\hat{v}_o}{dt} = D_{pv}^{'}\hat{\imath}_{Lpv} - I_{Lpv}\hat{d}_{pv} - \hat{\imath}_{opv} \\ C_{1pv}\dfrac{d\hat{v}_{pv}}{dt} = -\dfrac{1}{r_{pv}}\hat{v}_{pv} - \hat{\imath}_{Lpv} \end{cases} \quad (13)$$

where $i_{Lpv}$, $i_{opv}$, $r_{pv}$ and $d_{pv}$ are the inductor current, the output current, the output resistance of PV, the duty cycle for on-state of the switch, respectively. By considering the control diagram in Fig. 4, the small signal model in frequency domain is achieved

$$\hat{d}_{pv}(s) = -\hat{v}_{pv}^*(s)G_{pi7} + \hat{v}_{pv}(s)G_{pi7} \quad (14)$$

By analyzing the simultaneous equations of (13) and (14), it yields

$$\hat{v}_o(s) = G_{31}.\hat{v}_{pv}^*(s) - Z_{o2}.\hat{i}_{opv}(s) \quad (15)$$

where

$$\begin{aligned} & G_{31} = I_{Lpv}G_{pi7} - T_4 V_o G_{pi7}, Z_{o2} = \frac{1}{C_{2pv}s + T_4 D_{pv}^{\not c}} \\ & T_4 = \frac{D_{pv}^{\not c}(C_{2pv}s + 1/r_{pv}) + I_{Lpv}G_{pi7}}{1 + V_o G_{pi7} + L_{pv}s(C_{2pv}s + 1/r_{pv})} \end{aligned} \quad (16)$$

For the AC load connected to inverter, the analysis is presented in the next subsection.

### D. Small-Signal Model of The Inverter

The single-phase equation of a three-phase system can be obtained on the output side of the inverter, including the three-phase input voltage, the filter consists of an inductor and a capacitor, and the motor load is a resistive-inductive load as follows

$$\begin{cases} L_f\dfrac{di_{La}}{dt} = v_a - v_{ca} \\ C_f\dfrac{dv_{ca}}{dt} = i_{La} - i_{oa} \\ L_o\dfrac{di_{oa}}{dt} = v_{ca} - R_o i_{oa} \end{cases} \quad (17)$$

where $L_f$ , $C_f$ , $L_o$ , $R_o$ , $i_{La}$ , $v_a$ , $v_{ca}$ , and $i_{oa}$ are the filter

inductance, the filter capacitance, the load inductance, the load resistance, the filter inductance current, the filter capacitance voltage, the input voltage and the load current, respectively. According to Fig. 5 and using circuit laws, Park transformation, and Taylor series-based linearization, A state space representation can be given as follows

$$\begin{aligned} \dot{X} &= AX + B_1 \hat{v}_o \\ Y &= CX + D\hat{v}_o \end{aligned} \tag{18}$$

where

$$\begin{aligned} X &= \begin{bmatrix} \hat{i}_{Ld} & \hat{i}_{Lq} & \hat{v}_{cd} & \hat{v}_{cq} & \hat{i}_{od} & \hat{i}_{oq} & \hat{a}_1 & \hat{a}_2 & \hat{a}_3 & \hat{a}_4 \end{bmatrix}^T \\ B_1 &= \begin{bmatrix} \frac{M_d}{2L_f} & \frac{M_q}{2L_f} & 0 & 0 & 0 & 0 & 0 & 0 & 0 & 0 \end{bmatrix}^T \\ C &= \frac{3}{2V_o} \begin{bmatrix} 0 & 0 & I_{od} & I_{oq} & V_{cd} & V_{cq} & 0 & 0 & 0 & 0 \end{bmatrix} \\ D &= -\frac{I_{in,IN}}{V_o} \end{aligned} \tag{19}$$

By analyzing the simultaneous equations of (18) and (19), it yields

$$\hat{i}_{in,IN}(s) = \frac{1}{Z_{in,In}} \hat{v}_o(s) \tag{20}$$

where

$$Z_{in,IN} = \frac{\hat{v}_o}{\hat{i}_{in,IN}} = \left[ C\left(sI - A\right)^{-1} B_1 + D \right]^{-1} \tag{21}$$

By summarizing the results in (6), (11), (15) and (20), the small-signal model of the multistage configuration of electric vehicle is obtained, as shown in Fig. 6. The closed-loop transfer function between the main DC bus voltage and the load current is obtained as

$$TF(s) = \frac{\hat{v}_o(s)}{\hat{i}_{Load}(s)} = \frac{-1}{Z_{o1}^{-1} + Z_{o2}^{-1} + Z_{in,SC}^{-1} + Z_{in,IN}^{-1} + R_L^{-1}} \tag{22}$$

## IV. Stability Analysis and Parameter Selection

In this section, small-signal stability of the hybrid vehicle, is studied via analysis of the system eigenvalues using the transfer function derived in (22). Therefore, for AC load and the proposed control strategy, there are three parameters to be considered, namely, active power ($R_o$), virtual resistance ($R_v$), the virtual capacitance ($C_v$). The system parameters are given in Table I and Table II. The active power load connected to the inverter has a negative effect on the damping of the system. In Fig. 7, the eigenvalues of the entire system are plotted when $R_o$ decreases. By decreasing $R_o$, damping ratio of the complex conjugate eigenvalues ($\lambda_3$ and $\lambda_4$) continual decrease, so the system is more prone to low-frequency oscillation. The selected $R_o$ should ensure the stable operation of the whole system, i.e., all the dominant poles are located in left side of s domain. Therefore, the acceptable rang is $1.5 < R_o$. For load resistance values less than $R_o = 1.5\ \Omega$, the system becomes unstable. In Fig. 8(a), the eigenvalues of the entire system are plotted when $C_v$ increases. By increasing $C_v$, damping ratio of the complex conjugate eigenvalues ($\lambda_1$ and $\lambda_2$) continual decrease, so the system is more prone to low-frequency oscillation. The selected $C_v$ should ensure the stable operation of the whole system, i.e., all the dominant poles are located in left side of s domain. Therefore, the acceptable rang is $0 < C_v < 0.004$ (for $R_v = 8$). Fig. 8(b) shows the trajectory of dominant poles when $R_v$ decreases from 50 to 0.5. By increasing $1/R_v$, the damping factor of the system is improved. As it is observed, there is also an inflection point for the virtual resistance in the system root-locus diagram. Therefore, the inflection point of system root-locus will be the optimal one for $R_v$, namely, $R_v$=4.76.

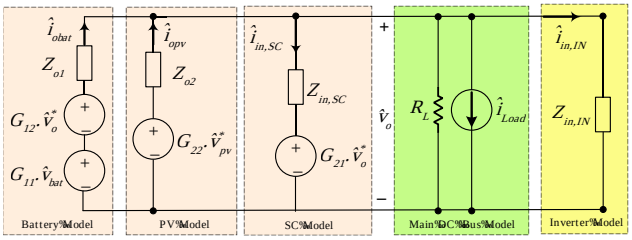


Fig. 6. Small-signal model of electric vehicle.

TABLE 1
SYSTEM PARAMETERS OF THE HYBRID VEHICLE

| system | Parameters | Values | Parameters | Values |
|---|---|---|---|---|
| *PV system* | $L_{pv}$ | 5mH | $v_{pv}$ | 109.4V |
| | $C_{1pv}$ | 0.1 mF | $C_{2pv}$ | 0.5mF |
| *Battery system* | $L_{bat}$ | 50 mH | $V_{bat}$ | 360V |
| | $C_{bat}$ | 0.1 mF | $V_{Cbat}$ | 800V |
| *SC system* | $L_{SC}$ | 10 mH | $V_{SC}$ | 250V |
| | $C_{SC}$ | 0.01 F | $C_{sc}$ | 0.5 mF |
| *Inverter* | $L_f$ | 5 mH | $v_{o,abc}$ | 220V-AC |
| | $C_f$ | 1 mF | $V_n$ | 311.12V |
| | $\omega_n$ | 100π | $m_p$ , $n_q$ | 0, 0 |
| *AC Load* | $L_o$ | 17.7 mH | $R_o$ | 28 Ω |
| *DC Load* | $R_L$ | 128Ω | Load power | 5 kW |

TABLE 2
CONTROLLER PARAMETERS OF THE HYBRID VEHICLE

| system | Parameters | Values | Parameters | Values |
|---|---|---|---|---|
| *Battery system* | $K_{p3}$ | 0.1 | $K_{i3}$ | 7 |
| | $K_{p4}$ | 0.1 | $K_{i4}$ | 30 |
| *SC system* | $K_{p5}$ | 0.6 | $K_{i5}$ | 5 |
| | $K_{p6}$ | 0.1 | $K_{i6}$ | 15 |
| *PV system* | $K_{p7}$ | 0.01 | $K_{i7}$ | 2 |
| *inverter* | $K_{p8}$ | 1 | $K_{i8}$ | 50 |
| | $K_{p9}$ | 1 | $K_{i9}$ | 30 |

## V. Simulation Results

In order to validate the effectiveness of the proposed virtual inertia control, the EV system, is simulated in MATLAB/Simulink. The system parameters can be found in Table I and Table II. The battery employs a bidirectional boost

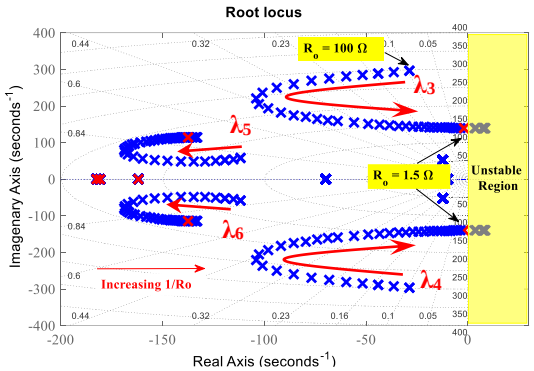
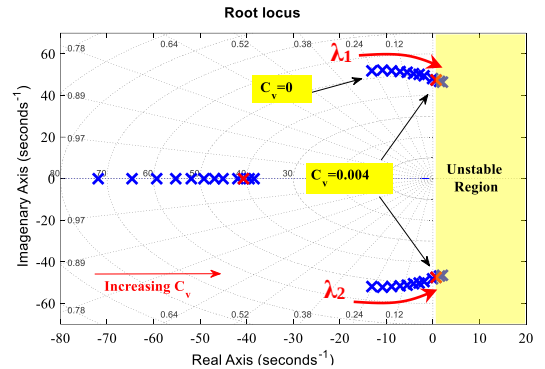
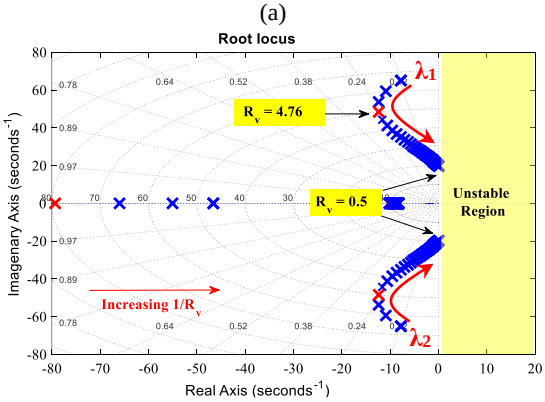



Fig. 7. Trace of the dominant poles for varying $R_o$



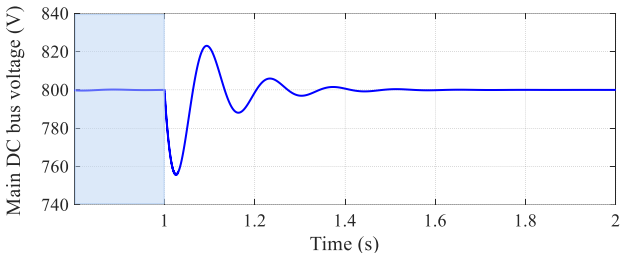

(a)



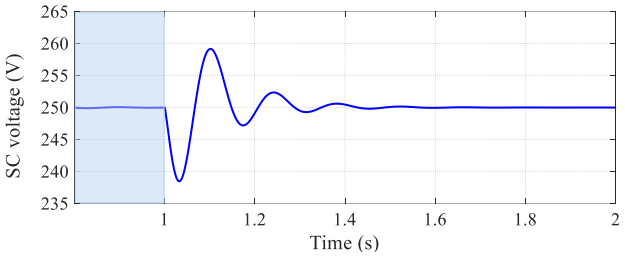

(b)

Fig. 8. Trace of the dominant poles for: (a) varying $C_v$ while $R_v$=8, (b) varying $R_v$ while $C_v$=0.001

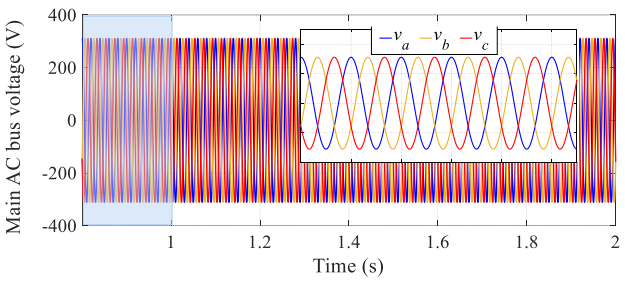
converter to establish the regulated main DC bus through control loops. The main DC bus and SC voltage are regulated at the rated value of 800 V and 250 V, respectively. It is assumed that a DC load with power rate of 5kW is directly connected to the main DC bus. the man AC bus is controlled at 220 V-rms and 50Hz and 5kW and 1 kvar AC load is connected to the main AC bus. Fig. 9 shows the main dc bus




(a)




(b)




(c)

Fig. 9. Voltage response based on proposed method to step changes in the DC load power: a) main DC bus voltage, b) SC voltage, c) main AC bus voltage.

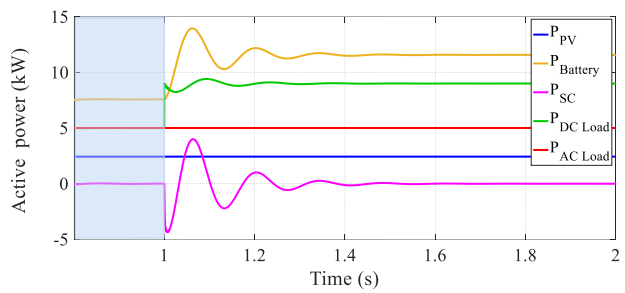



Fig. 10. Active power based on proposed method to step changes in DC load power.

voltage, SC voltage and main AC bud voltage when DC load power (at *t=1s*) changes. Fig. 10 shows the PV output power, battery output power, SC output power, DC load power and active power of AC load when DC load power changes. As can be seen, using the proposed virtual inertia ensures stable operation. To evaluate its effectiveness, a +80% change in DC load power from $P_{Load}$ = 5 kW to $P_{Load}$ = 9 kW at t=1s was investigated, with $C_v$=0.001 and $R_v$=4.76.

Fig. 11 shows the main DC bus voltage for varying in virtual inertia loop parameters. In Fig. 11 when *C*v and/or *1/R*v increase (decrease), the voltage deviation and RoCoV will

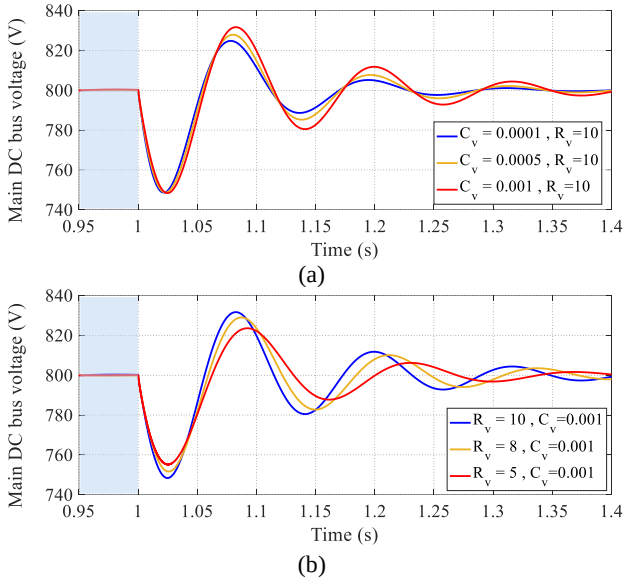



Fig. 11. Main DC bus voltage after a step change in load power, a) varying *Cv* for $R_v$=10, b) varying $R_v$ for *Cv* =0.001.

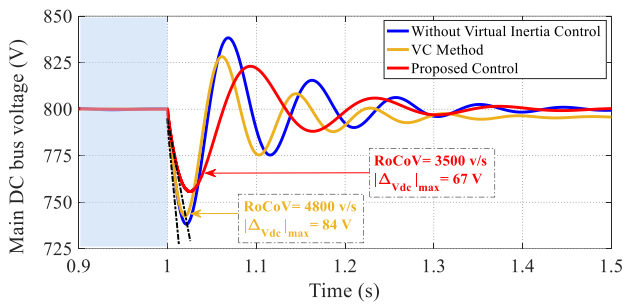



Fig. 12. Main DC bus voltage response based on basic, VC [27] and proposed methods.

decrease (increase), respectively. Meanwhile, the parameters of inertia response have no influence on the steady-state performance.

Fig. 12 compare the virtual capacitance (VC) method from [27] with the proposed virtual inertia loop method. Additionally, the result without an additional control loop is shown. Fig. 12 demonstrates that the virtual inertia controller improves the main dc bus voltage performance by reducing RoCoV, overshoot, and oscillations. This leads to an improved stability margin for the EV.

## VI. Conclusions

This paper presents a solution to address the issues of low inertia and significant dc bus voltage fluctuations in an EV due to limited system capacitance. The proposed approach involves implementing a virtual inertia control using an ESS based on SC. By introducing virtual capacitance, the inertia of the dc bus is increased, resulting in a reduction in the required capacitance and voltage drop in the EV. This is achieved by providing instantaneous current during step-load changes. The increase in virtual capacitance leads to a decrease in the RoCoV during variations in load power. However, it is important to note that a larger virtual capacitance can cause larger low-frequency oscillations and reduced damping. To mitigate this issue, a proportional feedback gain (1/*R*v) is implemented to mimic the damping factor and decrease the oscillations. This approach also improves the battery lifetime by reducing the rate of charge and discharge. A comprehensive small-signal model is derived, and the selection of parameters is discussed based on eigenvalues analysis. Simulation results demonstrate that the proposed method, which utilizes proportional-derivative feedback, outperforms other methods in terms of performance.

## References

[1] T. Mesbahi, P. Bartholomeus, N. Rizoug, R. Sadoun, F. Khenfri and P. Le Moigne, "Advanced model of hybrid energy storage system integrating lithium-ion battery and supercapacitor for electric vehicle applications," *IEEE Trans. Ind. Electron.*, vol. 68, no. 5, pp. 3962-3972, May 2021.

[2] A. K. Podder, O. Chakraborty, S. Islam, N. Manoj Kumar and H. H. Alhelou, "Control strategies of different hybrid energy storage systems for electric vehicles applications," *IEEE Access*, vol. 9, pp. 51865-51895, 2021.

[3] M. Carignano, V. Roda, R. Costa-Castelló, L. Valiño, A. Lozano, and F. Barreras, "Assessment of energy management in a fuel cell/battery hybrid vehicle," *IEEE Access*, vol. 7, pp. 16110-16122, 2019.

[4] A. Tahri, H. El Fadil, F. Z. Belhaj, K. Gaouzi, A. Rachid, F. Giri, and F. Z. Chaoui, "Management of fuel cell power and supercapacitor state-ofcharge for electric vehicles," *Electr. Power Syst. Res.*, vol. 160, pp. 89-98, Jul. 2018.

[5] S. Ahmadi, S. Bathaee, AH. Hosseinpour, "Improving fuel economy and performance of a fuel-cell hybrid electric vehicle (fuel-cell, battery, and ultracapacitor) using optimized energy management strategy," *Energy Conversion and Management*, vol. 160, pp. 74-84, 2018.

[6] J. P. Torreglosa, P. García, L. M. Fernández, and F. Jurado, "Predictive control for the energy management of a fuel-cell-battery-supercapacitor tramway," *IEEE Trans Ind. Informat.*, vol. 10, no. 1, pp. 276-285, Feb. 2014.

[7] S. Ahmadi and S. M. T. Bathaee, "multi-objective genetic optimization of the fuel cell hybrid vehicle supervisory system: Fuzzy logic and operating mode control strategies," *Int. J. Hydrogen Energy*, vol. 40, no. 36, pp. 12512-12521, Sep. 2015.

[8] J. Chen, C. Xu, C. Wu, and W. Xu, "Adaptive fuzzy logic control of fuel-cell battery hybrid systems for electric vehicles," *IEEE Trans. Ind. Informat.*, vol. 14, no. 1, pp. 292-300, Jan. 2018.

[9] L. Samaranayake and S. Longo, "Degradation control for electric vehicle machines using nonlinear model predictive control," *IEEE Trans. Control Syst. Technol.*, vol. 26, no. 1, pp. 89-101, Jan. 2018.

[10] M. H. K. Tushar, C. Assi, M. Maier, M. F. Uddin, "Smart Microgrids: optimal joint scheduling for electric vehicles and home appliances", *IEEE Trans. on Smart Grid*, vol. 5, no. 1, pp. 239 – 250, Jan. 2014.

[11] K. W. Hu, C. M. Liaw, "Incorporated Operation Control of DC Microgrid and Electric Vehicle", *IEEE Trans. on Ind. Electron*., vol. 63, no. 1, pp. 202 – 215, Jan. 2016.

[12] J. Fang, H. Li, Y. Tang, and F. Blaabjerg, "On the inertia of future more-electronics power systems," *IEEE J. Emerg. Sel. Topics Power Electron.*, vol. 7, no. 4, pp. 2130–2146, Dec. 2019.

[13] M. Su, Z. Liu, Y. Sun, H. Han, X. Hou, "Stability analysis and stabilization methods of DC microgrid with multiple parallel-connected DC–DC converters loaded by CPLs," *IEEE Trans. Smart Grid*, vol. 9, no. 1, pp.132-142, Mar. 2016.

[14] W. Yu, Z. Liu, and I. A. Tasiu, "Virtual inertia control strategy of traction converter in high-speed railways based on feedback linearization of sliding mode observer," *IEEE Trans. Veh. Technol.*, vol. 70, no. 11, pp. 11390–11403, Nov. 2021.

[15] G. Lin, J. Liu, C. Rehtanz, C. Li, Y. Li, and P. Wang, "Inertia droop control and stability mechanism analysis of energy storage systems for dc-busbar electric vehicle charging station," *IEEE Trans. on Transp. Electrific.*, vol. 9, no. 1, pp. 266-282, Mar 2023.

[16] H. Ali, "A hybrid energy storage system based on supercapacitor and electric vehicle batteries for frequency stability improvement of islanded microgrids," in *2022 23rd International Middle East Power Systems Conference (MEPCON)*, 2022, pp. 1-6.

[17] H. Jafari, M. Moghaddami, T. O. Olowu, A. Sarwat and M. Mahmoudi, "Virtual inertia-based multi-power level controller for inductive electric vehicle charging systems," *IEEE Trans. Emerg. Sel. Topics Power Electron.*, vol. 9, no. 6, pp. 7369-7382, Dec. 2021.

[18] L. Huang, H. Xin, H. Yuan, G. Wang, and P. Ju, "Damping effect of virtual synchronous machines provided by a dynamical virtual impedance," *IEEE Trans. Energy Convers.*, vol. 36, no. 1, pp. 570–573, Mar. 2021.

[19] A. Karimipouya, S. Karimi, H. Abdi, "Microgrid frequency control using the virtual inertia and ANFIS-based controller," *International Journal of Industrial Electronics, Control and Optimization*, vol. 2, no. 2, pp. 145-154, Apr. 2019.

[20] A. Karimi, Y. Jafarian, H. Bevrani, R. Mirzaei, "Frequency response improvement in microgrids: a fuzzy–based virtual synchronous generator approach," *International Journal of Industrial Electronics, Control and Optimization*, vol. 3, no. 2, pp.147-158, Apr. 2020.

[21] Y. Zhang, Q. Sun, J. Zhou, L. Li, P. Wang, and J. M. Guerrero, "Coordinated control of networked AC/DC microgrids with adaptive virtual inertia and governor-gain for stability enhancement," *IEEE Trans. Energy Convers.*, vol. 36, no. 1, pp. 95–110, Mar. 2021.

[22] Y. Yang, C. Li, J. Xu, F. Blaabjerg, and T. Dragiˇcevi´c, "Virtual inertia control strategy for improving damping performance of DC microgrid with negative feedback effect," *IEEE J. Emerg. Sel. Topics Power Electron.*, vol. 9, no. 2, pp. 1241–1257, Apr. 2021.

[23] Q. Ye, R. Mo, and H. Li, "Impedance modeling and DC bus voltage stability assessment of a solid-state-transformer-enabled hybrid AC–DC grid considering bidirectional power flow," *IEEE Trans. Ind. Electron.*, vol. 67, no. 8, pp. 6531–6540, Aug. 2020.

[24] W. Du, Q. Fu and H. F. Wang, "Small-signal stability of a DC network planned for electric vehicle charging," *IEEE Trans. Smart Grid*, vol. 11, no. 5, pp. 3748-3762, Sep. 2020.

[25] R. Shi, S. Semsar and P. W. Lehn, "Single-stage hybrid energy storage integration in electric vehicles using vector controlled power sharing", *IEEE Trans. Ind. Electron.*, vol. 68, no. 11, pp. 10623-10633, 2021.

[26] J.-L. Kuo, K.-L. Chao, and L.-S. Lee, "Dual mechatronic MPPT controllers with PN and OPSO control algorithms for the rotatable solar panel in PHEV system," *IEEE Transactions on Industrial Electronics*, vol. 57, no. 2, pp. 678–689, 2009.

[27] E. Unamuno, J. A. Barrena, "Design and small-signal stability analysis of a virtual-capacitor control for dc microgrids," *Proc. 19th Eur. Conf. Power Electron. Appl. (EPE ECCE Eur.)*, pp.1-10, 2017.



**Mehran Jami** was born in Marivan, Iran (1986). He received the B.Sc. degree from University of Tehran, Tehran, Iran, and the M.Sc. degree from Tarbiat Modares University (TMU), Tehran, Iran, and the Ph.D. degree from University of Kurdistan, Sanandaj, Iran, all in Power Electrical Engineering in 2012, 2014, and 2020 respectively. He is currently an Assistant Professor in the Department of Electrical Engineering, Islamic Azad University, Marivan Branch, Marivan, Iran. His research interests include modeling, analysis, design, and control of power electronic devices.